

Article

# Research on Precursor Information of Brittle Rock Failure through Acoustic Emission

Weiguang Ren <sup>1,2</sup> , Chaosheng Wang <sup>3,4,\*</sup>, Yang Zhao <sup>2</sup> and Dongjie Xue <sup>5</sup> <sup>1</sup> China Institute of Coal Science, Beijing 100013, China; rwgjszsj@outlook.com<sup>2</sup> China Coal Research Institute, Beijing 100013, China; zhao\_no1@126.com<sup>3</sup> School of Civil Engineering and Architecture, Henan University of Science and Technology, Luoyang 471023, China<sup>4</sup> Engineering Technology Research Center of Safety and Protection of Buildings of Henan Province, Luoyang 471023, China<sup>5</sup> School of Mechanics and Civil Engineering, China University of Mining and Technology Beijing, Beijing 100083, China; xuedongjie@163.com

\* Correspondence: 9905755@haust.edu.cn

**Abstract:** Dynamic failure of surrounding rock often causes many casualties and financial losses. Predicting the precursory characteristics of rock failure is of great significance in preventing and controlling the dynamic failure of surrounding rock. In this paper, a triaxial test of granite is carried out, and the acoustic emission events are monitored during the test. The fractal characteristics of acoustic emission events' energy distribution and time sequence are analyzed. The correlation dimension and the  $b$  value are used to study the size distribution and sequential characteristics. Furthermore, a rock failure prediction method is proposed. The correlation dimension is chosen as the main index and the  $b$  value is chosen as a secondary index for the precursor of granite failure. The study shows that: (1) The failure process can be divided into an initial stage, active stage, quiet stage, and failure stage. (2) The  $b$  value and correlation dimension both can describe the process of rock failure. There is a continuous decline before failure. Because of the complexity of the field, it is difficult to accurately estimate the stability of surrounding rock using a single index. (3) The combination of the  $b$  value and correlation dimension to establish a new method, which can accurately represent the stability of the surrounding rock. When the correlation dimension is increasing, the surrounding rock is stable with stress adjusting. When the correlation dimension is decreasing and the  $b$  value remains unchanged after briefly rising, the surrounding rock is stable, and stress is finished adjusting. When the correlation dimension and  $b$  value are both decreasing, the surrounding rock will be destroyed.

**Keywords:** granite; AE;  $b$  value; correlation dimension; precursor information**MSC:** 74L10

**Citation:** Ren, W.; Wang, C.; Zhao, Y.; Xue, D. Research on Precursor Information of Brittle Rock Failure through Acoustic Emission. *Mathematics* **2023**, *11*, 4210. <https://doi.org/10.3390/math11194210>

Academic Editors: Xin Cai, Shaofeng Wang, Yu Wang and Xueming Du

Received: 4 September 2023

Revised: 30 September 2023

Accepted: 7 October 2023

Published: 9 October 2023



**Copyright:** © 2023 by the authors. Licensee MDPI, Basel, Switzerland. This article is an open access article distributed under the terms and conditions of the Creative Commons Attribution (CC BY) license (<https://creativecommons.org/licenses/by/4.0/>).

## 1. Introduction

With the burial depth of underground engineering gradually increasing, underground engineering faces a complex geological environment, such as high geostress, high temperature, high pore pressure, and intense excavation disturbance, which lead to an irreversible development of internal defects within the rock. Brittle rock is a common rock in deep underground engineering. With damage accumulating, the surrounding brittle rock is prone to dynamic disasters such as rock bursts, which can seriously impact construction progress and project safety, and even result in numerous casualties and financial losses [1,2]. Revealing prospective predictions and implementing prompt measures constitute effective approaches to prevent and manage subterranean dynamic disasters in the surrounding geological formations [3–5]. Therefore, it is of great significance to study the precursor information of brittle rocks in order to prevent engineering disasters.

Acoustic emission (AE) is a phenomenon of transient elastic waves generated by the rapid release of energy from local sources in materials. AE can characterize the damage and pore-fracture evolution of rock samples under stress. The characteristics of AE can reflect the damage and failure state of rock. Therefore, acoustic emission technology is often used to monitor rock damage and failure in underground engineering [6,7]. The AE characteristics are closely related to the failure state of the rock, which indicates that the failure state of the rock can be predicted using AE characteristic parameters [8]. The analysis of AE signal characteristics mainly includes AE event number, energy and count, spatial localization, and fractal characteristics [9–11].

Many scholars revealed rock damage and failure characteristics based on AE characteristics. Vishal et al. [10] studied the mechanical behavior of coal under fluid saturation using AE characteristics. Moradian et al. [12] found that AE events could be used to describe the failure levels of brittle rocks. Shkuratnik et al. [13] studied the changes in the AE spectra of coal under uniaxial and triaxial compression tests and found that the AE spectral patterns vary greatly at the coal pre-failure stage under uniaxial compression tests. Abbas et al. [14] investigated the impact of high attenuation on rock AE mapping failure and then proposed a new method to monitor the rock failure position based on the AE events. Yang et al. [15] analyzed AE characteristics and fractal features of disc samples during splitting failure in relation to the loading rate. Holcomb [16] evaluated the stress state of surrounding rock based on the Kaiser effect principle of acoustic emission and applied AE event number to rock damage evaluation. Kusunose et al. [17] investigated the spatial distribution of acoustic emission events under triaxial testing conditions for two different texture distributions of granite.

Since Mandelbrot proposed the concept of fractal, fractal theory has attracted more and more attention from scientists and technologists in various fields [18]. Xie [19] expounded and proved fractures of rocks from microcracks to broken all have fractal characteristics, and the fractal dimension gradually reduces in the process of failure. So, the fractal method also received attention in the analysis of AE. Scholars have conducted AE experiments on the loading and unloading of rocks under various stress conditions and analyzed the fractal characteristics of AE events during the process of rock failure. Then, the fractal characteristic of AE events was applied to analyze the stress state or stable state of rock. The most common characterizing parameters are the AE  $b$ -value [20–23] and correlation dimension [24–26]. Many scholars have conducted extensive experimental research on the evolution of the  $b$ -value and correlation dimension under various stress conditions. The  $b$  value is related to the stress state of rocks, and it is negatively correlated with stress [27]. The fractal dimensions are lower in initial loading stages and increase gradually along with stress; about at 40% of the strength, fractal values begin to fall down [28]. With the development of research on fractal theory in AE, it has been verified that fractal parameters of AE can describe the precursor information of rock instability and failure. Virkar et al. [29] found that the  $b$  value could be used to predict rock failure and analyze rock damage. Hayakawa et al. [30] researched the AE fractal characteristic of cold forging tool damage during forming operation and calculated the AE fractal dimension of deformation and fracture, which verified that fractal dimension can be used to describe cold forging tool failure as an effective indicator. In summary, many domestic and foreign scholars have extensively investigated AE characteristics and precursor characteristics of rock failure. They proposed many methods to predict rock failure. But the methods cannot accurately predict the failure of rocks. Therefore, precursor characteristics based on the  $b$  value and correlation dimension under different confining pressures were investigated. The fractal characteristics of AE events' energy distribution and time sequence were analyzed. The application of laboratory experiment results in field construction was further discussed.

## 2. Samples and Experiment Method

### 2.1. Granite Samples

The samples were taken from the underground research laboratory (URL) of the Beishan preselected area of China’s high-level radioactive waste geological repository (Figure 1). The samples are classified into granodiorite, which is intact with a hard texture and has partial development of fissures. The Beishan granodiorite displays a hue ranging from white to grayish red. The rock mass remains undeformed or displays limited deformation. The rock mass primarily consists of a grained granite structure, exhibiting irregular and blocky textures. The main minerals in the samples are plagioclase (30–40%), potash feldspar (10–20%), quartz (20–30%), biotite (2–8%) and hornblende (1–3%) [31,32].

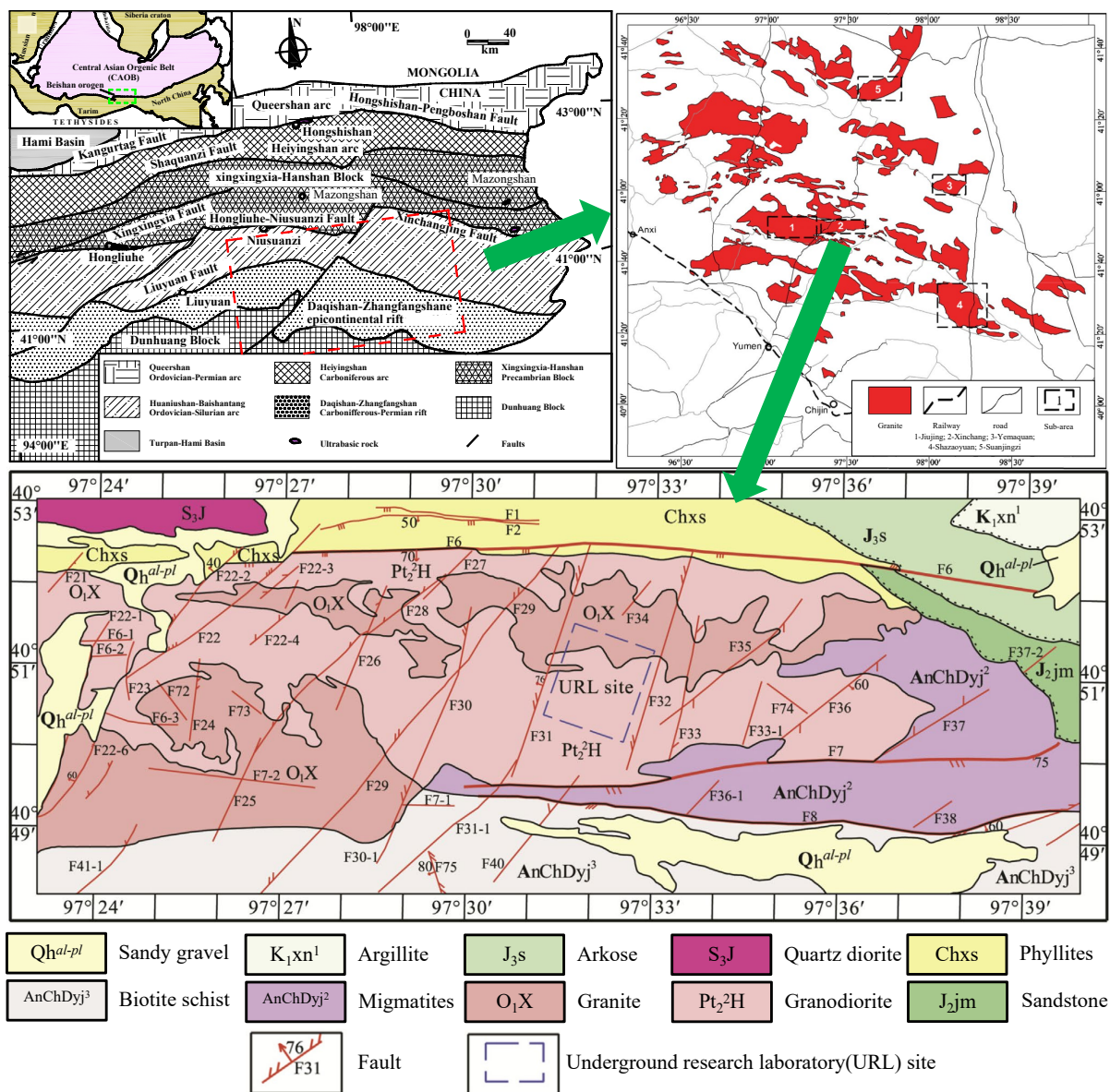


Figure 1. Geological map of the sampling site (URL site) [31,32].

The core cuttings were used for X-ray fluorescence spectroscopy analysis (XRF). Detailed information on the samples is listed in Table 1. According to XRF results, the samples contain SiO<sub>2</sub>, Al<sub>2</sub>O<sub>3</sub>, Fe<sub>2</sub>O<sub>3</sub>, MgO, CaO, Na<sub>2</sub>O, K<sub>2</sub>O, MnO, TiO<sub>2</sub>, P<sub>2</sub>O<sub>5</sub>, LOI, and FeO. The highest content is SiO<sub>2</sub>, which varies from 69.77% to 70.99%. The content of Al<sub>2</sub>O<sub>3</sub> varies from 14.78% to 15.19%. The content of Na<sub>2</sub>O, K<sub>2</sub>O, CaO, Fe<sub>2</sub>O<sub>3</sub>, and FeO are all less than

5%, varying from 3.66% to 4.77, 2.94% to 4.13%, 2.25% to 2.56%, 2.00% to 2.21%, and 1.57% to 1.70%, respectively. The content of MgO, LOI, TiO<sub>2</sub>, P<sub>2</sub>O<sub>5</sub>, and MnO are all less than 1%, varying from 0.77% to 0.81%, 0.66% to 0.89%, 0.323% to 0.376%, 0.091% to 0.100%, and 0.037% to 0.038%, respectively.

**Table 1.** Major elements in the samples/%.

Sample ID	SiO <sub>2</sub>	Al <sub>2</sub> O <sub>3</sub>	Fe <sub>2</sub> O <sub>3</sub>	MgO	CaO	Na <sub>2</sub> O	K <sub>2</sub> O	MnO	TiO <sub>2</sub>	P <sub>2</sub> O <sub>5</sub>	LOI	FeO
A	70.99	14.78	2.00	0.79	2.25	3.66	4.13	0.037	0.323	0.100	0.89	1.63
B	70.89	15.19	2.14	0.77	2.56	4.31	2.94	0.038	0.376	0.092	0.66	1.70
C	69.77	15.15	2.21	0.81	2.41	4.77	3.57	0.037	0.371	0.091	0.75	1.57

2.2. Experimental Detail

The triaxial compression experiments were conducted using an MTS815 Flex Test GT rock mechanics test system (Figure 2) manufactured in the United States. The AE events were recorded using a PCI-II Acoustic Apparatus manufactured by American Acoustics Company in the process of the experiment. The acquisition frequency of AE sensors was set to 200 kHz. The threshold value for signal acquisition was set to 26 dB. The layout of the AE sensors is shown in Figure 3. Each specimen is symmetrically arranged with 8 AE sensors. The eight AE sensors are evenly arranged on the upper and lower sections of the specimen. The center of the four AE sensors arranged on the bottom surface is the coordinate origin, with the z-axis direction upward and the x-axis and y-axis in the horizontal direction. The coordinates of each sensor are shown in Table 2.

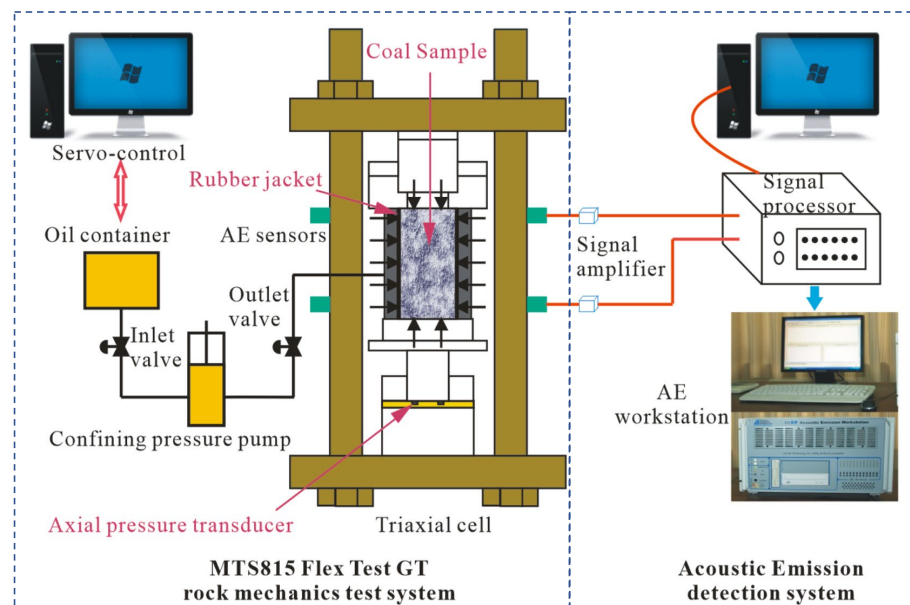


**Figure 2.** MTS815 Flex Test GT rock mechanics test system and the AE detection system.

**Table 2.** The coordinates of AE sensors.

Numbers	1	2	3	4	5	6	7	8
x (mm)	0	180	0	−180	0	180	0	−180
y (mm)	180	0	−180	0	180	0	−180	0
z (mm)	140	140	140	140	0	0	0	0

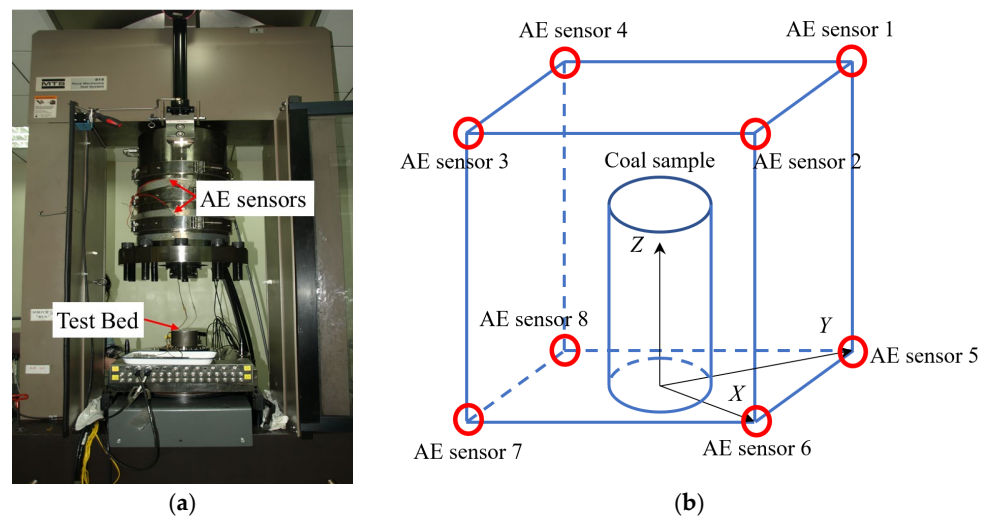


**Figure 3.** The layout of AE sensors: (a) experimental equipment and (b) spatial position of AE sensors.

Axial stress and circumferential deformation were combined to control loading. The specific experimental steps are as follows: (1) Axial force was applied to the sample with axial stress control at 30 KN/min. (2) The loading control changed from axial stress control to circumferential deformation control when the inflection point of the volume strain curve appeared. (3) Axial force was applied to the sample with circumferential deformation control at 0.02 mm/min until the specimen was damaged. During the experiments, the confining pressure was set to 5, 10, 15, and 30 MPa, respectively, according to the stress characteristics of Beishan and the depth of the underground laboratory.

### 2.3. AE Localization

The AE localization algorithm primarily consists of the simplex algorithm [33] and the Geiger algorithm [34]. Both algorithms calculate the position of an AE event by the time difference in sound emission signals received from different location sensors [35]. In this study, the Geiger algorithm is used to determine the location of the AE event for specimen failure. In the experiment, eight AE sensors are fixed in certain spatial positions, and their coordinates were assumed to be  $S_i (x_i, y_i, z_i)$  ( $i = 1, 2, 3, 4, 5, 6, 7, 8$ ). The relative time difference in picking up P-waves with different position sensors is measured to achieve spatial localization of the AE event. For an AE event, given the focal coordinates  $(x, y, z)$ , the initial time of the AE event  $t$ , and the arrival time  $t_i$  ( $i = 1, 2, 3, 4, 5, 6, 7, 8$ ) of P-wave received by sensor  $S_i$ , the location of the AE event can be calculated using the following equation.

$$(x_i - x)^2 + (y_i - y)^2 + (z_i - z)^2 = v^2(t_i - t)^2 \quad (1)$$

where  $v$  is the velocity of the P-wave in the travel path. In Equation (1), there exist four unknown variables  $(x, y, z, t)$ , which required at least four AE sensors triggered to determine the four unknown variables.

## 3. Experiment Results and Analysis

### 3.1. Experiment Results

Figure 4 shows stress–strain curves of the specimens under different confining pressures. The confining pressure of the 1–6, 1–7, 1–10, and 1–11 specimens were 5, 10, 15, and 30 MPa, respectively. The peak strength of the 1–6, 1–7, 1–10, and 1–11 specimens were 172.4, 218.8, 264.3, and 358.0 MPa, respectively. With the confining pressure increasing, the peak strength significantly increases. The specimens exhibit obvious shear failure (Figure 5). As the confining pressure increases, the specimen destruction is more intense, which means the energy release is more severe.

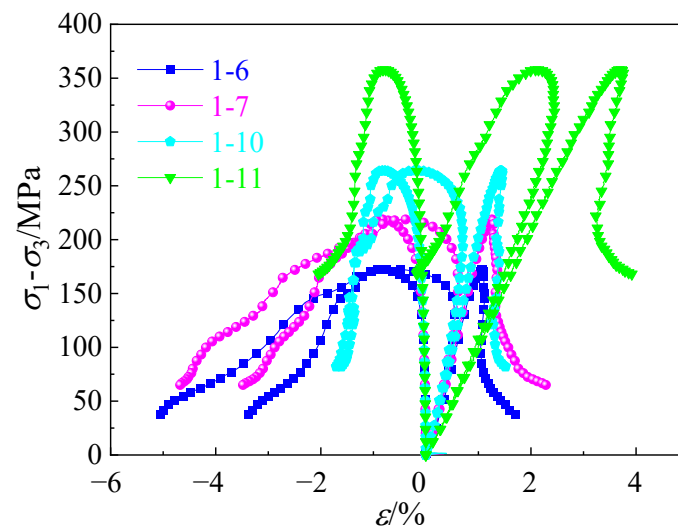


**Figure 4.** Stress—strain curves of specimen under different confining pressures.

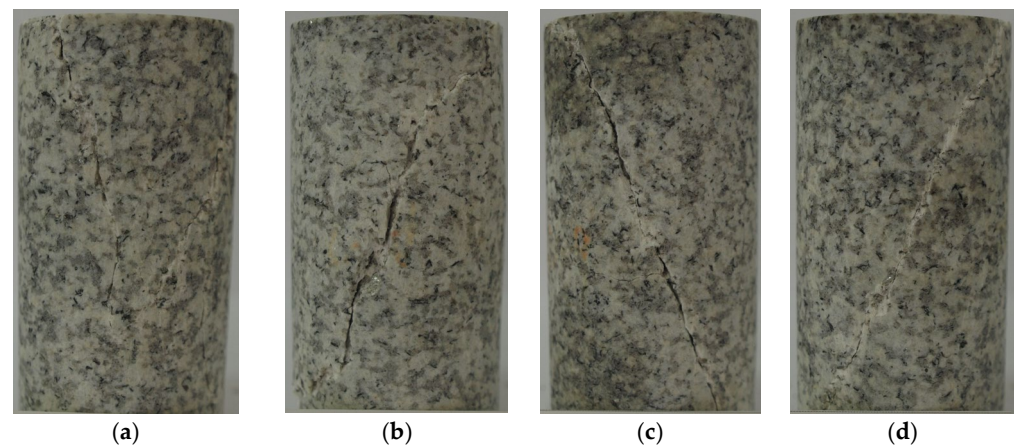


**Figure 5.** Image of failure specimens: (a) 1–6; (b) 1–7; (c) 1–10; and (d) 1–11.

### 3.2. Characteristics of AE

Figure 6 shows curves of AE hits, amplitude, and stress with time. The confining pressure of the 1–6, 1–7, 1–10, and 1–11 specimens were 5, 10, 15, and 30 MPa, respectively. According to the number of AE events, the failure process is divided into the initial stage, active stage, quiet stage, and failure stage (Figure 3, respectively, with I, II, III, IV).

The initial stage runs through the stage of compaction and elastic deformation of the specimen. AE events show a sporadic distribution and the number of AEs is small, so few fractures occur, and AEs mainly come from the original crack closing. The active stage begins with the stress being about 40% of the peak stress and finishes with stress reaching 98% of the peak stress. During this stage, a large number of fractures are generated, expanded, and connected, which is the main stage of crack generation and propagation. AE events in the quiet phase decreased sharply, mainly because more cracks had been already generated and the stress was redistributed at the crack tip. During this period, the expansion of cracks is primarily driven by small-scale fractures. During the failure stage, stress concentrates on the rupture surface, and the fracture further expands so that AE events rapidly increase.

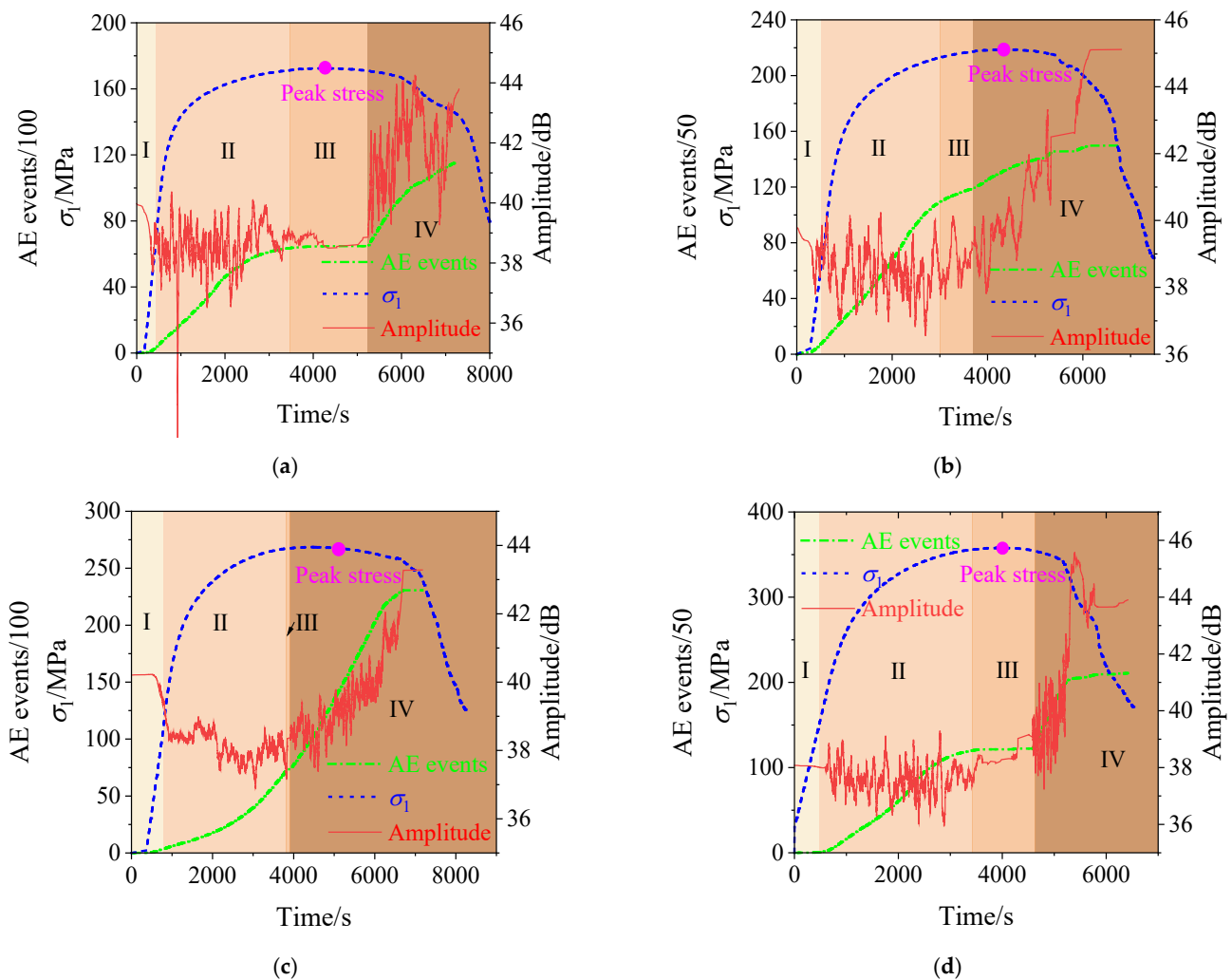


**Figure 6.** Curves of AE hits, AE amplitude, and stress with time: (a) 1–6; (b) 1–7; (c) 1–10; and (d) 1–11.

As shown in Figure 5, the amplitude of each specimen showed a stable decrease in the initial stage and its fluctuation was not obvious. The amplitude in the active stage fluctuated obviously, but the overall trend in amplitude remained constant. In the quiet stage, the amplitude fluctuation of the 1–6, 1–10, and 1–11 specimens disappeared, and their size basically remained stable, which was obviously different from the active phase. However, the amplitude of specimen 1–7 in the calm stage showed little difference from that in the active stage.

In summary, AEs in the process of failure can be divided into four stages, AEs in different stages have different characteristics, and the quiet period can provide some reference for rock failure. Due to the inhomogeneity in the rock, AE characteristics in the quiet stage are not obvious at times, such as the AE event number of the 1–7 specimen. So, it is hard to capture the quiet stage before failure because the duration of the quiet period is very short. Therefore, AE characteristics can provide some references for rock failure, but they cannot provide an accurate destruction of precursor information.

### 3.3. Research on the $b$ Value

In this paper, the G-R relationship and the G-P algorithm [36] are used to study the distribution characteristics and sequential features of AE energy, respectively. The method for calculating the AE  $b$  value using the G-R relationship is shown in Equation (2).

$$\lg N = a - b \lg Q \quad (2)$$

where  $Q$  is absolute energy contained in an AE event,  $N$  is the number of AE events whose energy is greater than or equal to  $Q$ ,  $a$  and  $b$  are constants, and the physical meaning of the AE  $b$  value is a measure of development of the crack.  $b$  values and their change trends are closely related to the development of cracks in the rock.

When the  $b$  value decreases, the proportion of small AE events decreases, and the proportion of large AE events increases. On the contrary, the proportion of small events increases. When the  $b$  value changes slowly or its amplitude is small, the number of large events and small events is stable, and crack development is a gradual and stable expansion. A significant reduction in  $b$  indicates that the evolution of cracks is drastic and is a symbol of dramatic increasing in AE events, which may cause damage to the rock. In this paper, the  $b$  value was counted every 500 AE events, and  $\lg N$  and  $\lg Q$  were fitted to linear (Figure 7).

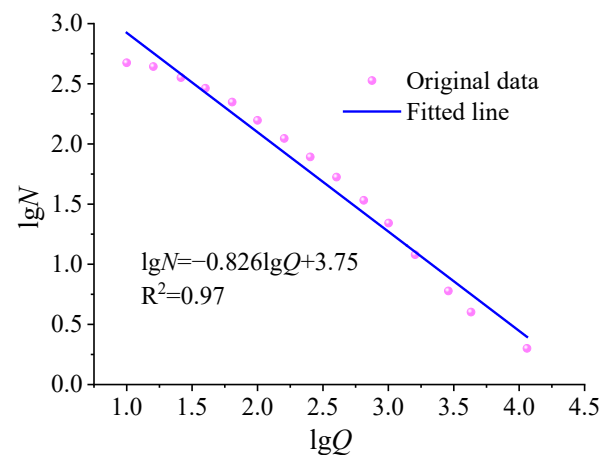


**Figure 7.** Fitting curve of  $\lg N$  and  $\lg Q$ .

The relationship between the  $b$  value, stress, and time is shown in Figure 8 and Table 3. From Figure 8 and Table 3, it can be seen that the  $b$  value of AE basically shows an upward trend before the stress reaches damage stress, which indicates AE events are dominated by small events and the fracture propagates slowly. In the unstable crack expansion stage, the  $b$  value begins to fluctuate, indicating that small AE events and large events alternately occupy the leading position; therefore, the rapid expansion of large fractures and the slow expansion of small fractures alternately dominate the internal rock fracture expansion. However, in the process, the  $b$  value does not change much, which shows that the fractures gradually and steadily expand inside the rock. In the later stage of unstable fracture expansion, the  $b$  value generally showed a steady downward trend, and the specimen quickly reached the peak and failure, which shows that the proportion of AE events increased, and large cracks developed rapidly before failure.

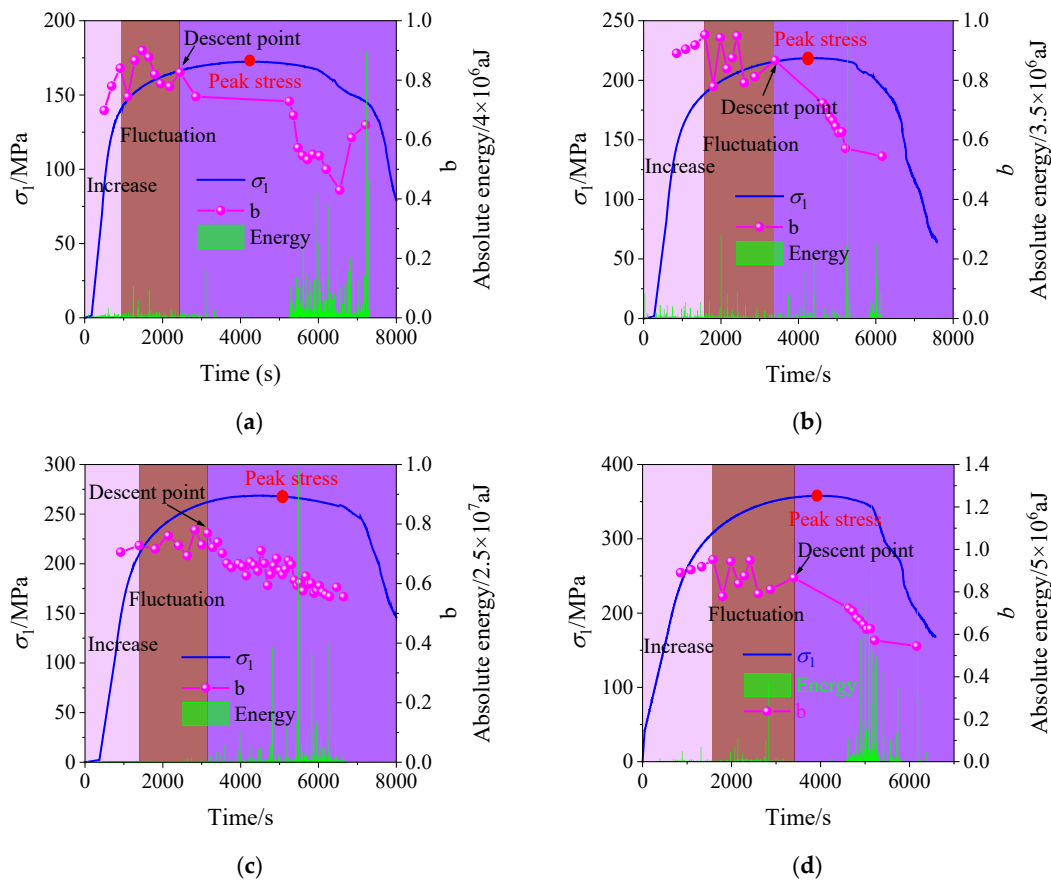


**Figure 8.** Curves of the  $b$  value, AE energy, and stress with time: (a) 1–6; (b) 1–7; (c) 1–10; and (d) 1–11.

**Table 3.** Relationship between  $b$  and time.

Number	$b$ Value	Time/s	Stress/MPa
1–6	increase	0–913	0–139.88
	fluctuation	913–250	139.88–166.80
	descent point	2500	166.80
1–7	increase	0–1393	0–182.83
	fluctuation	1393–3300	182.83–215.32
	descent point	3300	215
1–10	increase	0–1214	0–194
	fluctuation	1214–3150	194.21–262.85
	descent point	3150	262
1–11	increase	0–1582	0–308.14
	fluctuation	1582–3400	308.14–353.42
	descent point	3400	353.42

The peak stress of specimens 1–6, 1–7, 1–10, and 1–11 appear at 4260, 4310, 5060, and 3900 s, respectively, and the  $b$ -value descent point is 1760, 1110, 1910, and 500 s earlier than the peak stress. The  $b$ -value descent point is in the later stage of unstable crack expansion, the stress of the  $b$ -value descent point is relatively large, but it is less than peak stress. Therefore, the  $b$ -value steady descent point can be chosen as a precursor of rock failure.

### 3.4. Research on the Correlation Dimension

The AE correlation dimension is an AE fractal dimension calculated using the G-P relationship [36]. In this method, a multi-dimensional space is reconstructed based on the temporal feature of the AE parameter. Considering the coordinates  $p_i$  of AE events as individual elements and arranging the AE events in a time sequence, a coordinate set of AE events can be obtained.

$$\begin{cases} A = \{p_1, p_2, \dots, p_n\} \\ p_i = \{x_i, y_i, z_i\} \end{cases} \tag{3}$$

Select a positive integer  $m$  ( $m < n$ ). Then, an  $m$ -dimensional phase space for AE events in the time sequence can be established.

$$\begin{cases} P_1 = \{p_1, p_2, \dots, p_m\} \\ P_2 = \{p_2, p_3, \dots, p_{m+1}\} \\ \dots \\ P_{n-m+1} = \{p_{n-m+1}, p_{n-m+2}, \dots, p_n\} \end{cases} \tag{4}$$

For the constructed  $m$ -dimensional phase space, the correlation function can be defined under a given scale  $r$ .

$$C(r) = \frac{1}{N^2} \sum_{i=1}^N \sum_{j=1}^N H(r - \langle P_i - P_j \rangle) \tag{5}$$

where  $H(x)$  is the Heaviside function.  $\langle P_i - P_j \rangle$  represents the distance between two  $m$ -dimensional phase space points.

$$H(x) = \begin{cases} 1, & x > 0 \\ 0, & x \leq 0 \end{cases} \tag{6}$$

$$\langle P_i - P_j \rangle = \left[ \sum_{t=1}^m (P_{i,t} - P_{j,t})^2 \right]^{\frac{1}{2}} \tag{7}$$

The correlation function represents the proportion of AE events with spatial distance less than the scale  $r$  in the total. The scale  $r$  can be obtained using the following equation.

$$r = k \frac{1}{N^2} \sum_{i=1}^N \sum_{j=1}^N \langle P_i - P_j \rangle \tag{8}$$

where  $k$  is the proportional coefficient. In this study,  $k$  was selected as 0.1, 0.2, 0.3, 0.4, 0.5, 0.6, 0.7, 0.8, 0.9, 1.0, 1.1, 1.2.  $N$  is the number of  $m$ -dimensional phase space points.

The correlation dimension can be determined using the correlation function and the scale. Applying logarithms to the correlation function and the scale, there is a linear relationship between  $\lg C(r)$  and  $\lg r$ . The slope is the correlation dimension.

$$D = \lim_{r \rightarrow 0} \frac{\lg C(r)}{\lg r} \tag{9}$$

where  $D$  is the correlation dimension, which represents the concentration of AE events in the reconstructed multi-dimensional space. The larger the  $D$  value is, the more concentrated the AE events are in the reconstructed multi-dimensional space. In this paper, the dimension value  $m$  of the phase space was 15, and the delay time was 1 s. The correlation dimension was calculated every 500 s. The linear fitting of  $\lg r$  and  $\lg C(r)$  is shown in Figure 9.

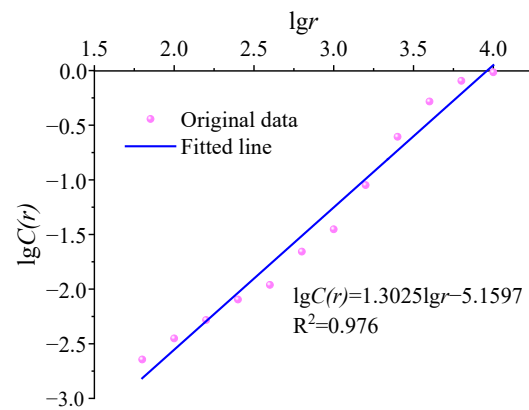


Figure 9. Fitting curve of  $lgr$  and  $lgC(r)$ .

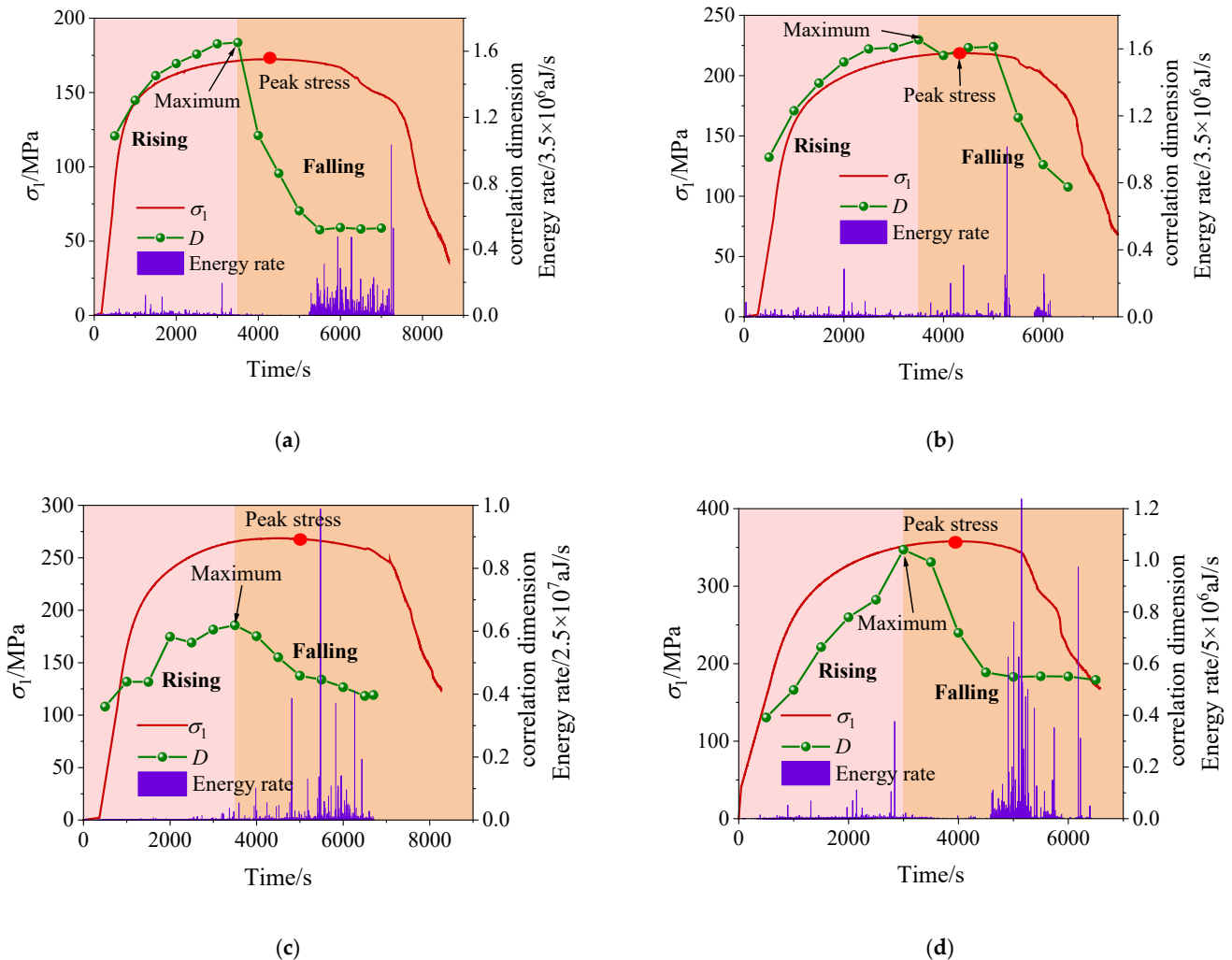
The correlation dimension initially rises and then falls throughout the experiment (Table 4 and Figure 10), which can be divided into two distinct stages: rising and falling. The maximum correlation dimensions for specimens 1–6, 1–7, 1–10, and 1–11 occurred at time points of 3500 s, 3500 s, 3500 s, and 3000 s, respectively. The rising stage encompasses the period from the beginning of loading to reaching the maximum correlation dimension. During this stage, there is an increase in the ratio of AE event pairs with short distances, indicating a progressive concentration of AE events in the reconstructed multi-dimensional space. Additionally, the stable AE energy rate suggests a stable expansion of cracks within the granite sample. Subsequently, the correlation dimension reaches its peak value before continuously declining during the falling stage, which extends from reaching a maximum correlation dimension to sample failure. In this stage, there is an increase in the ratio of AE event pairs with long distances, signifying the dispersion of AE events in the reconstructed multi-dimensional space. Notably, both the value and time sequence of AE energy rate exhibit significant fluctuations during this period suggesting unstable expansion behavior of cracks within granite.

Table 4. Relationship between correlation dimension and time.

Number	Correlation Dimension	Time/s	Stress/MPa
1–6	Rising	0–3500	0–171.23
	Maximum	3500	171.23
	Falling	3500–7000	171.23–156.87
1–7	Rising	0–3500	0–216.54
	Maximum	3500	216.54
	Falling	3500–6500	216.54–179.62
1–10	Rising	0–3500	0–265.41
	Maximum	3500	265.41
	Falling	3500–6700	265.41–256.18
1–11	Rising	0–3000	0–351.72
	Maximum	3000	351.72
	Falling	3000–6500	351.72–175.31

The correlation dimension continuously declines during the falling stage. In this stage, main failures initially appeared locally, resulting in abnormal AE energy rates in terms of both numerical values and time sequences. Consequently, the correlation dimension declines. Subsequently, microcracks form and connect these localized main failures. During this period, the number and energy rate of AE events are relatively low, leading to a continuous decline in the correlation dimension. Finally, as the connectivity between localized main failures increases, cracks rapidly expand and form a major failure surface in the specimen. The AE events generated during this period exhibit abrupt timing and high

energy rates. The correlation dimension continues to decrease accordingly. The maximum correlation dimensions of 1–6, 1–7, 1–10, and 1–11 appear at 3500 s (760 s earlier than the peak stress point), 3500 s (830 s earlier than the peak stress point), 3500 s (1560 s earlier than the peak stress point), and 3000 s (900 s earlier than the peak stress point), respectively. Therefore, the correlation dimension can also be considered as precursor information for rock failure.



**Figure 10.** Curves of the correlation dimension, energy rate, and stress with time: (a) 1–6; (b) 1–7; (c) 1–10; and (d) 1–11.

**4. Discussion**

The *b* value and correlation dimension calculated based on AE events both can well describe the fracture propagation and failure process in rock. They all decrease before specimen destruction, which indicates that rock failure is a process of dimension reduction and dissipation. The *b* value and correlation dimension both can be used as effective indicators to evaluate the stability of rock masses and provide advanced warning signals. The *b* value fluctuates for a long time before continuously falling, so it is difficult to determine the decent point. The change in the correlation dimension is relatively simple, which only has rising and falling stages in the entire destruction process. However, a sudden increase or decrease in the AE energy rate can lead to the correlation dimension decreasing, and the reason for the decrease usually cannot be determined. In summary, the correlation dimension is chosen as the main index, and the *b* value is chosen as a secondary index for the precursor of rock failure. The surrounding rock stability state has the following three kinds of situations (Figure 11).

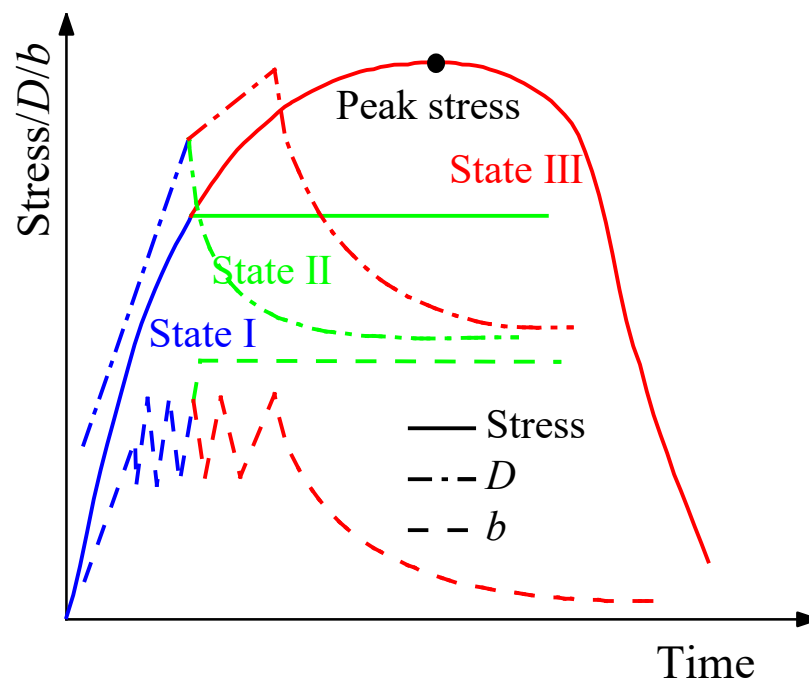


Figure 11. Sketch of the relationship between stable state, fractal dimension,  $b$ , and stress.

- (1) Surrounding rock stress is redistributing, and damage continuously increases with increasing stress, which is similar to the active stage in laboratory experiments. In this situation, the correlation dimension continually increases, and the  $b$  value keeps fluctuating after a short increase (State I in Figure 11).
- (2) Stress redistribution has been completed. But the surrounding rock is still in a stable state and does not produce AE events anymore. Most AE events received during this state are high-frequency noise events. Both the AE energy rate and events are reduced suddenly, and the proportion of small events increases. The correlation dimension suddenly drops, but the  $b$  value remains unchanged after a short rise (State II in Figure 11).
- (3) The surrounding rock stress is redistributing again. As the stress increases, the surrounding rock is gradually destroyed, which is similar to a complete laboratory experiment. This situation has a significant impact on engineering safety. Therefore, it is necessary to predict the stability of the surrounding rock in advance before the surrounding rock destruction. The correlation dimension and  $b$  value continuously decrease before rock failure, which has been validated using laboratory experiments. So, it is necessary to take some measures to avoid the occurrence of dynamic disasters when the correlation dimension and  $b$  value both decrease (State III in Figure 11).

In summary, the comprehensive correlation dimension and  $b$  value can simply and accurately characterize the different stability of the surrounding rock and further warn of the destruction of the surrounding rock. It is necessary to calculate the correlation dimension and  $b$  value from time to time and always pay attention to their change during tunneling. When the correlation dimension remains unchanged or increases, the surrounding rock is still in the process of stress adjustment and is in a stable state. When the correlation dimension and the  $b$  value decrease at the same time, the surrounding rock will be destroyed, and protective measures need to be taken. When the correlation dimension decreases and the  $b$  value remains stable after a brief rise, the stress adjustment in the surrounding rock is complete, and the surrounding rock is still in a relatively stable state.

## 5. Limitations and Future Works

In this paper, the AE characteristics of specimens are studied in detail. However, the physical properties and the deformation characteristics of specimens were not mentioned, which is important to study rock failure [37]. In this paper, the correlation dimension is chosen as the main index, and the  $b$  value is chosen as the secondary index for the precursor of granite failure. However, the method is still in the laboratory stage and has not been verified on-site. In future works, the physical properties and the deformation characteristics will be studied using theoretical analysis, physical experiments, and numerical simulation, focusing on the investigation of failure evolution in a specimen, which can be studied using nuclear magnetic resonance, micro-X-ray computed tomography, and so on. In future works, the method for the precursor of granite failure proposed in this article will be verified and applied in an engineering site. Based on the experimental results of the engineering site, the predictive indicators will be further quantified and analyzed. Then, quantitative indicators will be proposed.

## 6. Conclusions

This study conducted triaxial compressive tests of granite specimens and monitored AE signals during the experiments. AE fractal characteristic parameters were studied. The AE  $b$  value and correlation dimension were calculated using the G-P algorithm, which was used to predict the precursor information of rock failure. The conclusions are as follows.

- (1) The rock failure process can be divided into the initial stage, active stage, quiet stage, and failure stage based on the characteristics of AE events. During the quiet stage, the number of AE events is very few and the amplitude remains in a constant state. The quiet stage can be selected as a precursor information of rock failure.
- (2) The AE  $b$  value and correlation dimension both can describe the rock failure process and show a continuous decline before destruction. But the  $b$  value fluctuates for a long time before continuously falling. A sudden increase or decrease in the AE energy rate can lead to a decrease in the correlation dimension, and the reason for the decrease usually cannot be determined.
- (3) Regarding the comprehensive correlation dimension and  $b$  value, the correlation dimension is chosen as the main index, and the  $b$  value is chosen as the secondary index for the precursor of rock failure, which can simply and accurately evaluate the different stability of the surrounding rock and further warn of the destruction of the surrounding rock.

**Author Contributions:** Conceptualization, W.R.; methodology, W.R. and C.W.; validation, Y.Z. and D.X.; formal analysis, C.W.; investigation, Y.Z. and D.X.; resources, W.R. and C.W.; data curation, C.W. and Y.Z.; writing—original draft preparation, W.R.; writing—review and editing, C.W.; visualization, Y.Z.; supervision, W.R. and D.X.; project administration, Y.Z.; funding acquisition, W.R., C.W., Y.Z. and D.X. All authors have read and agreed to the published version of the manuscript.

**Funding:** This work was supported by the National Natural Science Foundation of China (Grant Nos. 52104082), the Science and Technology Development Fund Project of China Coal Research Institute (Grant Nos. 2021CX-II-12 and 2022CX-I-04), Science and Technology Project of China Energy Investment Corporation (CEIC) (GJNY2030XDXM-19-01.2, GJNY-21-42) and the Open Fund of State Key Laboratory of Water Resource Protection and Utilization in Coal Mining (GJNY-20-113-04).

**Data Availability Statement:** Not applicable.

**Conflicts of Interest:** The authors declare no conflict of interest.

## References

1. Akdag, S.; Karakus, M.; Nguyen, G.D.; Taheri, A.; Bruning, T. Evaluation of the propensity of strain burst in brittle granite based on post-peak energy analysis. *Undergr. Space* **2019**, *6*, 1–11. [[CrossRef](#)]
2. Zhou, Z.; Cai, X.; Li, X.; Cao, W.; Du, X. Dynamic Response and Energy Evolution of Sandstone Under Coupled Static–Dynamic Compression: Insights from Experimental Study into Deep Rock Engineering Applications. *Rock Mech. Rock Eng.* **2020**, *53*, 1305–1331. [[CrossRef](#)]

3. Xie, H.; Gao, F.; Ju, Y. Research and development of rock mechanics in deep ground engineering. *Chin. J. Rock Mech. Eng.* **2015**, *34*, 2161–2178.
4. Bieniawski, Z.T. Mechanism of brittle rock fracture: Part 1—Theory of the fracture process. *Int. J. Rock Mech. Min. Sci. Geomech. Abstr.* **1967**, *4*, 395–406. [[CrossRef](#)]
5. Sueyoshi, K.; Kitamura, M.; Lei, X.; Katayama, I. Identification of fracturing behavior in thermally cracked granite using the frequency spectral characteristics of acoustic emission. *J. Mineral. Petrol. Sci.* **2023**, *118*, 221014. [[CrossRef](#)]
6. Lockner, D.A.; Byerlee, J.D.; Kuksenko, V.; Ponomarev, A.; Sidorin, A. Quasi-static fault growth and shear fracture energy in granite. *Nature* **1991**, *359*, 39–42. [[CrossRef](#)]
7. Thompson, B.D.; Young, R.P.; Lockner, D.A. Observations of premonitory acoustic emission and slip nucleation during a stick slip experiment in smooth faulted Westerly granite. *Geophys. Res. Lett.* **2005**, *32*, 10304. [[CrossRef](#)]
8. Vilhelm, J.; Vladimír, R.; Tomáš, L.; Živor, R. Application of autocorrelation analysis for interpreting acoustic emission in rock. *Int. J. Rock Mech. Min. Sci.* **2008**, *45*, 1068–1081. [[CrossRef](#)]
9. Rudajev, V.; Vilhelm, J.; Lokajcek, T. Laboratory studies of acoustic emission prior to uniaxial compressive rock failure. *Int. J. Rock Mech. Min. Sci.* **2000**, *37*, 699–704. [[CrossRef](#)]
10. Vishal, V.; Ranjith, P.G.; Singh, T.N. An experimental investigation on behaviour of coal under fluid saturation, using acoustic emission. *J. Nat. Gas Sci. Eng.* **2015**, *22*, 428–436. [[CrossRef](#)]
11. Ishida, T.; Kanagawa, T.; Kanaori, Y. Source distribution of acoustic emissions during an in-situ direct shear test: Implications for an analog model of seismogenic faulting in an inhomogeneous rock mass. *Eng. Geol.* **2010**, *110*, 66–76. [[CrossRef](#)]
12. Moradian, Z.; Einstein, H.H.; Ballivy, G. Detection of cracking levels in brittle rocks by parametric analysis of the acoustic emission signals. *Rock Mech. Rock Eng.* **2016**, *49*, 785–800. [[CrossRef](#)]
13. Shkuratnik, V.L.; Nikolenko, P.V.; Koshelev, A.E. Spectral characteristic of acoustic emission in loaded coal specimens for failure prediction. *J. Min. Sci.* **2017**, *53*, 818–823. [[CrossRef](#)]
14. Abbas, H.A.; Mohamed, Z.; Kudus, S.A. Anisotropic AE Attenuation in Mapping of Composite Specimen Progressive Failure under Unconfined Loading. *Int. J. Geomech.* **2023**, *23*, 04023005. [[CrossRef](#)]
15. Yang, J.; Zhao, K.; Song, Y.; Yan, Y.; He, Z.; Zhou, Y.; Gu, S. Acoustic emission characteristics and fractal evolution of rock splitting and failure processes under different loading rates. *Arab. J. Geosci.* **2022**, *15*, 265. [[CrossRef](#)]
16. Holcomb, D.J. General theory of the Kaiser effect. *Int. J. Rock Mech. Min. Sci. Geomech. Abstr.* **1993**, *30*, 929–935. [[CrossRef](#)]
17. Kusunose, K.; Lei, X.; Nishizawa, O.; Satoh, T. Effect of grain size on fractal structure of acoustic emission hypocenter distribution in granitic rock. *Phys. Earth Planet. Inter.* **1991**, *67*, 194–199. [[CrossRef](#)]
18. Mandelbrot, B.B. *The Fractal Geometry of Nature*; Freeman: San Francisco, CA, USA, 1983.
19. Heping, X. *Introduction to Fractal Rock Mechanics*; Science Press: Beijing, China, 1996.
20. Gutenberg, B.; Richter, C.F. Frequency of earthquakes in California. *Bull. Seismol. Soc. Am.* **1944**, *34*, 185–188. [[CrossRef](#)]
21. Dong, L.; Zhang, L.; Liu, H.; Du, K.; Liu, X. Acoustic Emission b Value Characteristics of Granite under True Triaxial Stress. *Mathematics* **2022**, *10*, 451. [[CrossRef](#)]
22. Smith, W.D. The b-value as an earthquake precursor. *Nature* **1981**, *289*, 136–139. [[CrossRef](#)]
23. Schroeder, M. *Fractals, Chaos, Power Laws: Minutes from an Infinite Paradise*; W. H. Freeman: New York, NY, USA, 1991.
24. Costin, L.S. A microcrack model for the deformation and failure of brittle rock. *J. Geophys. Res. Solid Earth* **1983**, *88*, 9485–9492. [[CrossRef](#)]
25. Kong, X.; Wang, E.; Hu, S.; Shen, R.; Li, X.; Zhan, T. Fractal characteristics and acoustic emission of coal containing methane in triaxial compression failure. *J. Appl. Geophys.* **2016**, *124*, 139–147. [[CrossRef](#)]
26. Carpinteri, A.; Lacidogna, G.; Niccolini, G. Fractal analysis of damage detected in concrete structural elements under loading. *Chaos Solitons Fractals* **2009**, *42*, 2047–2056. [[CrossRef](#)]
27. Scholz, C. The frequency-magnitude relation of microfracturing in rock and its relation to earthquakes. *Bull. Seismol. Soc. Am.* **1968**, *58*, 399–415. [[CrossRef](#)]
28. Yin, X.G.; Li, S.L.; Tang, H.Y.; Pei, J.L. Study on quiet period and its fractal characteristics of rock failure acoustic emission. *Chin. J. Rock Mech. Eng.* **2009**, *28*, 3383–3390.
29. Virkar, Y.; Clauset, A. Power-Law Distributions in Empirical Data. *Siam Rev.* **2009**, *51*, 661–703. [[CrossRef](#)]
30. Hayakawa, K.; Nakamura, T.; Yonezawa, H.; Tanaka, S. Detection of damage and fracture of forging die by fractal property of acoustic emission. *Mater. Trans.* **2004**, *45*, 3136–3141. [[CrossRef](#)]
31. Shan, L. *Triassic Granitoids in Beishan-Inner Mongolia, China and Its Tectonic Implications*; Chinese Academy of Geological Sciences: Beijing, China, 2013.
32. Wang, J.; Chen, L.; Su, R.; Zhao, X. The Beishan underground research laboratory for geological disposal of high-level radioactive waste in China: Planning, site selection, site characterization and in situ tests. *J. Rock Mech. Geotech. Eng.* **2018**, *10*, 411–435. [[CrossRef](#)]
33. Nelder, J.A.; Mead, R. A Simplex Method for Function Minimization. *Comput. J.* **1964**, *7*, 308–313. [[CrossRef](#)]
34. Geiger, L. Probability method for the determination of earthquake epicenters from the arrival time only. *Bull. St. Louis Univ.* **1912**, *8*, 60–71.
35. Spence, W. Relative epicenter determination using P-wave arrival-time differences. *Bull. Seismol. Soc. Am.* **1980**, *70*, 171–183.

36. Grassberger, P.; Procaccia, I. Characterization of strange attractors. *Phys. Rev. Lett.* **1983**, *50*, 346–349. [[CrossRef](#)]
37. Cai, X.; Yuan, J.; Zhou, Z.; Tan, L.; Wang, P.; Wang, S.; Wang, S. Effects of hole shape on mechanical behavior and fracturing mechanism of rock: Implications for instability of underground openings. *Tunn. Undergr. Space Technol.* **2023**, *141*, 105361. [[CrossRef](#)]

**Disclaimer/Publisher’s Note:** The statements, opinions and data contained in all publications are solely those of the individual author(s) and contributor(s) and not of MDPI and/or the editor(s). MDPI and/or the editor(s) disclaim responsibility for any injury to people or property resulting from any ideas, methods, instructions or products referred to in the content.